Applied Catalysis B: Environmental 142–143 (2013) 849–860

Contents lists available at SciVerse ScienceDirect

Applied Catalysis B: Environmental

journal homepage: www.elsevier.com/locate/apcatb

PtNi supported on oxygen functionalized carbon nanotubes: In depth structural characterization and activity for methanol electrooxidation

Abu Bakr Ahmed Amine Nassr[a,1], Ilya Sinev[b], Wolfgang Grünert[b], Michael Bron[a,*]

[a] Martin-Luther-Universität Halle-Wittenberg, Naturwissenschaftliche Fakultät II, Institut für Chemie, von-Danckelmann-Platz 4, 06120 Halle (Saale), Germany
[b] Ruhr-Universität Bochum, Lehrstuhl für Technische Chemie, Fakultät für Chemie und Biochemie, Bochum, Germany

ARTICLE INFO

Article history:
Received 19 January 2013
Received in revised form 13 June 2013
Accepted 17 June 2013
Available online 22 June 2013

Keywords:
Functionalized CNTs
PtNi electrocatalyst
Polyol reduction
Methanol electrooxidation
XAFS

ABSTRACT

Mild-condition nitric acid functionalized carbon nanotubes were used as support for PtNi electrocatalysts with variation of Pt to Ni atomic ratio prepared by a polyol method in which ethylene glycol was used as solvent and reducing agent under conventional reflux conditions. TPD, TGA, N_2 adsorption and cyclic voltammetry confirmed the presence of functional groups in the functionalized carbon nanotubes. Supported PtNi nanocatalysts were characterized with ICP-OES, TEM, XRD, XPS and XAFS. Well dispersed particles on the supporting material with particle sizes in the range of 2–3 nm were obtained. PtNi alloy formation was concluded from XRD, XPS and XAFS results, while the latter two methods point to the formation of Ni oxides as well. The elemental distribution within the catalyst nanoparticles is inhomogeneous with Ni enrichment close to the support. Heat treatment in inert gas up to 400 °C results in restructuring of the catalysts surface which changes the active sites arrangements. CV and CO stripping measurements showed that the PtNi catalysts have a higher electrocatalytic activity toward methanol oxidation in comparison to a commercial Pt/C E-TEK catalyst and the highest activity was found for a Pt to Ni atomic ratio of 3. The prepared catalysts show highly stable mass specific activity over 200 potential cycles. The catalysts treated at higher temperature (400 °C) show a surface enriched in Pt and exhibit lower activity for methanol oxidation reaction but higher stability over 200 cycles. The high catalytic activity and durability of the prepared PtNi electrocatalysts render them possible candidate catalysts for methanol oxidation in direct methanol fuel cells (DMFCs).

1. Introduction

Direct methanol fuel cells (DMFCs) working with methanol as liquid fuel have received significant attention in the last decade. DMFCs are considered as an important alternative power sources for many applications such as portable devices. Methanol as organic liquid fuel has advantageous features including easy and safe handling, storage and transportation, high energy density as well as low cost [1–3]. However, despite these benefits, DMFCs are characterized by a significantly lower power density and lower efficiency than PEMFCs operating with hydrogen because of the slow oxidation kinetics of methanol and methanol crossover from the anode to the cathode [1–3].

Pt is the best catalyst for partial methanol electrooxidation but its poisoning by CO produced as intermediate during the methanol oxidation retards the complete oxidation process and lowers the activity for methanol oxidation on the Pt electrode surface. In this regard, substantial research has been conducted to improve the activity of Pt catalysts toward methanol oxidation [4–9]. The addition of a second metal or a metal oxide as promoter for CO oxidation is considered as one of the best ways to solve the problem of CO adsorption on the Pt surface [10–21]. In bimetallic systems, Pt can initiate the methanol oxidation reaction through adsorption-dehydrogenation steps and the second metal or metal oxide can supply the oxygen species which are needed to oxidize the adsorbed CO molecules and liberate the Pt surface for further methanol adsorption/oxidation [22–25]. This mechanism is known as the bifunctional mechanism and was suggested by Wantabe and Motoo [25]. Another mechanism called the ligand effect or the electronic effect has been proposed, according to which the second metal modifies the electronic properties of the Pt by charge transfer processes and lowers the adsorption energy of CO onto the Pt surface [22,26–28]. A broad variety of bimetallic systems such as

* Corresponding author. Tel.: +49 345 5525900; fax: +49 345 5527163.
E-mail address: michael.bron@chemie.uni-halle.de (M. Bron).
[1] On leave from Electronic Materials Research Department, Institute of Advanced Technology and New Materials, City for Scientific Research and Technological Applications (SRTA-City), Alexandria, Egypt.

0926-3373/$ – see front matter © 2013 Elsevier B.V. All rights reserved.
http://dx.doi.org/10.1016/j.apcatb.2013.06.013

PtRu, PtNi, PtSn and PtCo with improved activity for methanol oxidation have been studied to replace the monometallic Pt catalysts [10–15,29–37].

Among these bimetallic catalyst systems, PtNi has the promising characteristics of being resistant to dissolution in the potential range used for methanol electrooxidation due to the stability of Ni in the Pt lattice [27,38]. A passivating role of nickel oxides has also been postulated [27]. This dissolution process is observed in various bimetallic catalyst systems like PtRu. Also, Ni is very cheap in comparison to Ru which is a precious metal [32].

PtNi catalysts supported on carbon back have been reported as active catalysts for methanol electrooxidation in alkaline and acid media [27,28,38,39]. Nickel oxyhydroxides, which form through reversible redox reaction from nickel hydroxide or present as Ni component in Ni containing catalysts are also known to catalyze the methanol oxidation [40,41]. Furthermore, these mixed oxides, beside their corrosion resistance and stability under methanol oxidation conditions, provide mixed protonic and electronic conductivity which may facilitate the charge transfer during the oxidation process.

Park et al. [27] prepared PtNi and PtRuNi catalysts and studied their electrocatalytic activity toward methanol oxidation in acid media compared to Pt and PtRu with PtNi and PtRuNi showing higher activity than Pt and PtRu. They attributed the activity enhancement to an electronic effect, where Ni modifies the electronic properties of Pt and weakens the CO adsorption on the PtNi surface, and to the presence of nickel oxides which can participate in the oxidation reaction by hydrogen spillover. The electronic effect was detected from the shift of binding energy of Pt in PtNi as measured by XPS [27]. The enhancement of methanol oxidation through hydrogen spillover by nickel oxides has been also suggested by Liang et al. [42] for carbon supported PtRuNi prepared by microwave pulsed technique followed by reductive annealing, but they also suggest that the oxyhydroxide species can participate in oxidation of CO adsorbed on Pt surface which can be considered as type of a bifunctional mechanism. Density functional theory (DFT) studies on PtNi clusters confirmed the electronic modification of Pt by charge transfer from Ni to Pt leading to weakening of the adsorption of CO on PtNi clusters as estimated from the calculation of CO adsorption energy on PtNi clusters of different compositions [28].

Despite the above observations still work is needed to improve the catalytic activity of the PtNi catalyst system and to gain further insight into catalyst structure. In the literature, little work has been devoted to carbon nanotubes supported PtNi catalysts for methanol oxidation in acid media [43]. We report in this paper on the preparation of PtNi supported on CNTs with different atomic ratio of Pt to Ni by a polyol method using ethylene glycol as reducing agent. The prepared PtNi catalysts have been characterized with physical techniques to elucidate their structural features, while their electrochemical properties have been studied with CV and CO stripping to evaluate their electrocatalytic activity toward methanol electrooxidation reaction in acid media. Furthermore, heat treatment to liberate the catalysts from possible residual carbon species deposited during preparation resulted in significant changes in structure as well as catalytic behavior, which has been analyzed as well.

2. Experimental

2.1. Carbon nanotubes functionalization

Carbon nanotubes (CNTs) (Baytubes C 150 P) purchased from Bayer Material Science AG (Germany) were functionalized using nitric acid to introduce surface oxygen-containing groups. 500 mg of the as-received CNTs were dispersed in 100 ml of 5 M HNO_3 for 0.5 h under stirring followed by ultrasonication for 0.5 h. Then the mixture was refluxed using an oil bath at 100 °C for 6 h under stirring. After the reflux process, the mixture was left to cool to room temperature, diluted with 200 ml of deionized water and kept stirring overnight to hydrolyse the functional groups. The functionalized carbon nanotubes were separated by centrifugation and subjected to several washing cycles with deionized water until the pH of the washing water did not change anymore. Finally, the functionalized CNTs were dried in oven at 110 °C overnight and then crushed in a mortar into fine powder and stored in plastic vials until used. Throughout this paper the functionalized CNTs will be labeled FCNTs.

2.2. Characterization of functionalized carbon nanotubes

TPD was carried out with a Belcat B (Bel Inc., Japan) in which the FCNTs sample was heated under He gas and the released gases were detected with a mass spectrometer QMS GAM 400 (IPI; Germany). First a stream of He gas was passed over the sample for 1 h at 30 °C. Then the temperature was raised to 1000 °C with a ramp of 5 K min^{-1} at a gas flow rate of 30 ml min^{-1}.

TGA analysis was carried out with a SDT 2960 Simultaneous DTA-TGA, TA Instruments, USA, in oxygen atmosphere to determine the thermal stability and the purity of CNTs. The sample first was heated up to 100 °C at a heating rate of 20 K min^{-1} under nitrogen and dried at this temperature for 1 h. After cooling to 40 °C under nitrogen atmosphere, the sample was heated under oxygen atmosphere up to 800 °C at a heating rate of 5 K min^{-1}.

The textural properties (surface area and pore size, pore volume) of the CNTs before and after functionalization were determined by N_2 adsorption using a Sorptomatic 1900, Carlo ERBA. The sample was degassed at 120 °C for 24 h under vacuum followed by adsorption of nitrogen at 77 K.

The electrochemical behavior of the as-received and functionalized carbon nanotubes was tested with cyclic voltammetry in N_2-purged 0.5 M H_2SO_4 at a scan rate of 0.1 V/s in the potential window from −0.2 to 1.0 V (Ag/AgCl/sat. KCl) for 100 cycles and the last cycle was used for comparison.

2.3. Preparation of electrocatalysts

PtNi electrocatalysts supported on functionalized carbon nanotubes (PtNi/FCNTs) with different nominal atomic ratios and a targeted metal loading of 20 wt% were prepared using a polyol method in which ethylene glycol (EG) served as solvent and reducing agent at the same time. Typically, 100 mg of FCNTs were dispersed in 10 ml EG under stirring for 15 min. The required volumes of 0.0197 M $Ni(NO_3)_2{\cdot}6H_2O$ and of 0.0197 M H_2PtCl_6 in EG to prepare PtNi with different nominal atomic ratios of Pt:Ni (1:1, 2:1, 3:1, 3:2) were added dropwise under stirring followed by addition of 20 ml of EG and further intense stirring for 15 min. After that, the pH of the mixture was adjusted to 11 with 2 M NaOH/EG solution and sonicated in an ultrasonic bath for 15 min. To carry out the reduction of the metal salt, the mixture was refluxed in an oil bath at 160 °C for 6 h after which it was allowed to cool down to room temperature under stirring and the solid product was separated by centrifugation. After several cycles of washing with water and centrifugation to remove residual EG and to clean the catalyst surface from undesired anions like Cl^- and NO_3^-, the catalyst was dried in an oven overnight at 80 °C, crushed in a mortar into fine powder and kept in a glass vial.

For heat treatment, 20–25 mg catalyst was weighted in a quartz boat and inserted in a horizontal high temperature oven (GERO, Germany) equipped with a quartz tube. The tube was flushed with N_2 (purity 99.999%) for 30 min to remove oxygen before raising

the temperature with a heating ramp of 10 °C min^{-1} to 200 and 400 °C, respectively. After 2 h it was allowed to cool down to room temperature under N_2 atmosphere.

During this text, the PtNi/FCNTs catalysts will be labeled according to their nominal Pt to Ni atomic ratio and heat treatment temperature. For example, PtNi(3:1)/FCNTs 200 refers to a Pt to Ni ratio of 3 to 1 and a heat treatment at 200 °C. Otherwise, PtNi/FCNTs without any label refers in general to all PtNi catalysts prepared in this work without heat treatment.

2.4. Characterization of electrocatalysts

2.4.1. Structural characterization

Bulk compositions (metal loading and elements ratio) of the catalysts were determined with inductively coupled plasma-optical emission spectrophotometry (ICP-OES, Jobin Yvon Ultima 2, Horiba). The catalysts were subjected to digestion in aqua regia under microwave heating using a microwave reactor (micro PREP 1500 (MWS Vertriebs-GmbH, Leutkirch, Germany). The dissolved metals were separated from CNTs by filtration and diluted with water and then their concentrations were measured using ICP-OES. For verification, a commercial 20% Pt/C catalyst from E-TEK was subjected to the same analysis.

X-ray diffraction measurements were done using a D8 advanced X-ray diffractometer, Bruker AXS, working with a Cu Kα source (λ = 0.15406 nm) and collected for all prepared catalysts in the 2θ range from 20° to 90° at a scan rate of 2° min^{-1}.

TEM analysis was carried out with a LEO 912 (Japan) working at an acceleration voltage of 120 keV. The samples were prepared by dispersing the catalysts in ethanol and sonicating for a short time. Drops of this dispersion were deposited onto carbon coated copper girds and dried before analysis.

XPS measurements were done with a Leybold-Heraeus LH10 spectrometer equipped with an EA 10/100 multi-channel detector (Specs), with a base vacuum of 10^{-9} Torr. The data were collected at room temperature. Survey spectra were recorded with a step size of 1 eV and a sampling time of 0.1 s, whereas selected regions (Pt 4f, Ni 2p, C 1s and O 1s) were recorded with a step size of 0.1 eV and a varying sampling time. Mg Kα (1253.6 eV, at 12 kV and 20 mA) radiation was used for the excitation. The major C 1s photoemission line was used as an internal standard for energy calibration, with BE = 284.5 eV. For every sample two XPS measurements were done – in the as prepared state and after sputtering for 1 h with He^+ ions with 2 keV energy.

Data reduction and signal shape analysis were performed using the program package CASA XPS. Prior to peak fitting, the X-ray satellites were deconvoluted out of the spectra. Atomic ratios of elements were calculated from intensity ratios using the Scofield photoionization cross-section data together with an experimentally derived response function of the spectrometer to the variation of the photoelectron kinetic energy. The Pt area was determined by simple integration employing a Shirley-type background in a preselected binding energy (BE) window.

X-ray absorption fine structure (XAFS) measurements (Ni K-edge, 8333 eV, Pt L3-edge, 11,564 eV) were carried out at HASYLAB (DESY, Hamburg, Germany) at the beamline C using a double-crystal Si(1 1 1) monochromator, which was detuned to 65% of maximum intensity to exclude higher harmonics in the X-ray beam. The spectra were recorded in transmission mode at liquid nitrogen temperature. For the measurements ca. 120 mg of sample were pressed in a self supporting pellet (13 mm diameter) and wrapped with Kapton tape. All spectra were measured simultaneously with the reference spectrum of a Ni or Pt foil placed between second and third ionization chambers which allowed absolute energy calibration. The spectra of Ni and Pt foils, the corresponding oxides and platinum chloride, which were used as references, were collected under the same conditions. All spectra were measured 2 times to ensure their reproducibility.

Analysis of the EXAFS spectra was performed with the software VIPER for Windows [44]. In the spectra of the absorption coefficient μ, a Victorian polynomial was fitted to the pre-edge region for background subtraction. A smooth atomic background μ_0 was evaluated using a smoothing cubic spline. The Fourier analysis of the k^2-weighted experimental function $\chi = (\mu - \mu_0)/\mu_0$ was performed with a Kaiser window. The required scattering amplitudes and phase shifts were calculated by the ab initio FEFF8.10 code [45] for Ni metal hcp, NiO cubic, Pt metal fcc, and tetragonal P/4mmm Pt–Ni alloy structures. The fitting was done in the *k*- and *r*-spaces. The shell radius *r*, coordination number *N*, Debye–Waller factor σ^2 and adjustable "muffin-tin zero" ΔE were determined as fitting parameters. The errors of the fitting parameters were found by decomposition of the statistical χ^2 function near its minimum, taking into account maximal pair correlations.

2.4.2. Electrochemical characterization

All catalysts were tested toward methanol electrooxidation using cyclic voltammetry (CV). The experiments were carried out in a three compartment electrochemical cell using an Autolab PGSTAT128N potentiostat/galvanostat and a Pt electrode, an Ag/AgCl/sat. KCl electrode and a catalyst coated glassy carbon (GC) electrode as counter electrode, reference electrode and working electrode, respectively. The working electrode was prepared as follows: first, the GC electrode was polished to a mirror finish using alumina suspension (1 μm, 0.3 μm) sequentially with a polishing cloth and then ultrasonically cleaned in a mixture of ethanol:water = 1:1 (v/v) and deionized water for 10 min, respectively. To prepare the catalyst inks, 2.5 mg of PtNi/FCNTs or Pt/C were dispersed in 350 μl of a mixture of 5 wt% Nafion solution and isopropyl alcohol (1:6, v/v). The catalyst suspension was sonicated for 1 h in an ultrasonic bath and then stirred for 2 h. 5 μl of this suspension was dropped on the surface of the previously polished GC electrode with a geometrical area of 0.155 cm^2 and left to dry in air at room temperature.

To test electrocatalytic activity the prepared electrode was subjected to activation and surface cleaning by potential cycling for 100 cycles in an N_2 purged solution of 0.5 M H_2SO_4 at a scan rate of 0.1 V/s in the potential window of −0.2 to 1.0 V (Ag/AgCl/sat. KCl), then the activated electrode was subjected to 200 potential cycles under the same conditions in a 0.5 M H_2SO_4/1 M CH_3OH solution purged previously with N_2 for 20 min. The cycle number 20 was used to compare the electrocatalytic activities; however the development of activity with cycle number was also studied.

The electrochemical surface area (ECSA) was determined using CO stripping voltammetry in 0.5 M H_2SO_4 solution. The electrode was subjected to the same activation and cleaning procedures as mentioned above. Afterward, CO gas was purged into the cell for 20 min while keeping the potential at −0.15 V and then N_2 gas was purged for 20 min to remove the dissolved CO in the solution and finally the stripping voltammogram was recorded in the potential window of −0.15 to 0.9 V at a scan rate of 20 mV/s for 3 cycles. All potential in this article are measured and reported against an Ag/AgCl/sat. KCl electrode.

3. Results and discussion

3.1. Characterization of the functionalized support

To confirm the success of the functionalization process and to study the thermal stability of the functionalized carbon nanotubes, the FCNTs were characterized with temperature-programmed

desorption (TPD), thermal gravimetric analysis (TGA), nitrogen physisorption and cyclic voltammetry. The results are detailed in the Supplementary Information (SI) and are summarized here only briefly.

It is well known that the main groups created by nitric acid oxidation of carbon materials are oxygen containing groups, mainly carboxylic acid, lactone, anhydride, quinone and hydroxyl groups [46–49]. These groups are decomposing at different temperatures to release CO and CO_2. Thus, desorption of these gases at defined temperatures refers to the presence of specific surface groups. TPD analysis (Fig. 1 in supplementary information: Fig. SI1) confirms that various kinds of oxygen containing groups have been created on the CNTs surface upon their treatment with nitric acid. These surface oxygen groups may serve as anchoring sites for metal nanoparticles and enhance their dispersion on the FCNTs surface.

The thermal stability of CNTs in oxygen atmosphere was studied using TGA analysis. Fig. SI2 shows the TGA of as received and functionalized CNTs. The most significant observation is that the complete decomposition of the as received CNTs starts at 450 °C while for the FCNTs the complete decomposition starts at 500 °C, indicating their higher oxidative stability. This result could be explained by removal of some remnants of the metal catalyst used for CNT preparation during the functionalization with nitric acid. The presence of theses metal impurities could enhance the oxidation of as received nanotubes in O_2 atmosphere. Indeed, the residue remaining after TGA is higher for the as received CNTs (1.38%) than for the FCNTs (0.18%). Furthermore, amorphous carbon species, which should be burned at much lower temperatures [50], are obviously not formed during the mild nitric acid treatment.

The electrochemical properties of functionalized and as received CNTs were tested with cyclic voltammetry as shown in Fig. SI3. The functionalized carbon supports exhibit strong redox peaks in the forward and backward scans, which are characteristic for electroactive surface oxygen groups and assigned to hydroquinone-quinone redox couple (HQ/Q), while the as received CNTs do not show this behavior [51,52], confirming that the functionalization process was able to create oxygen surface functional groups on the CNT surface.

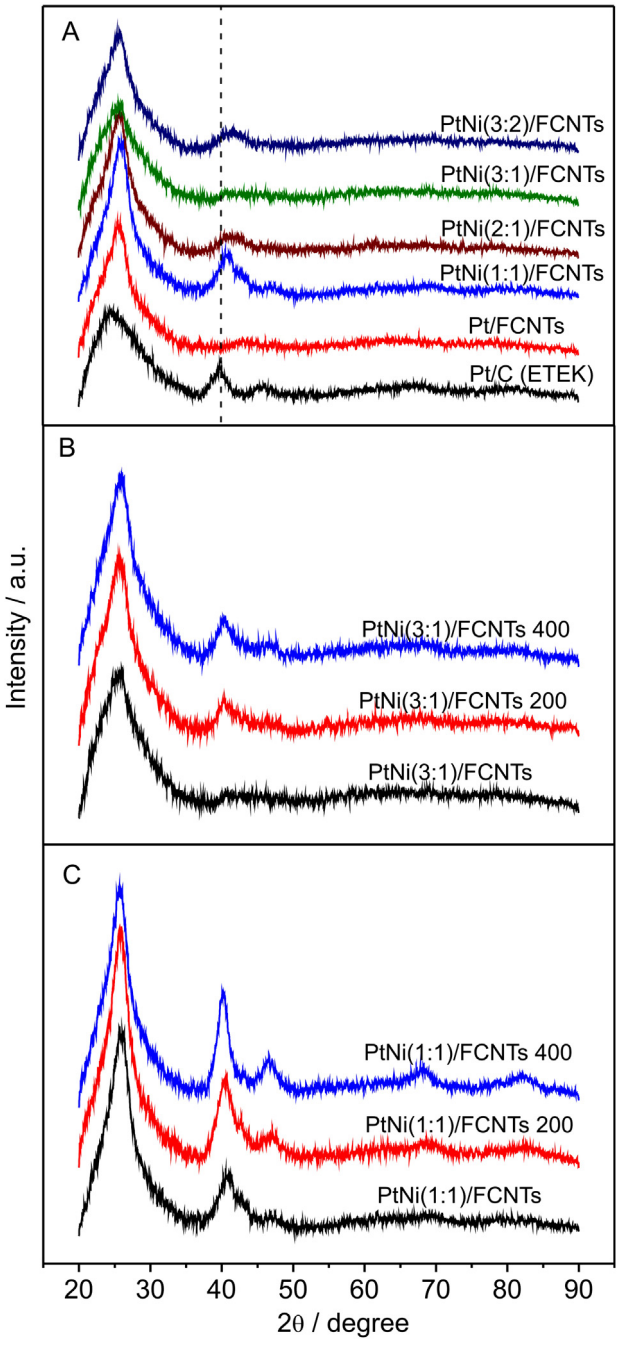

Fig. 1. XRD patterns of Pt/C (ETEK), Pt/FCNTs and PtNi/FCNTs electrocatalysts (A), heat treated PtNi(3:1)/FCNTs (B) and PtNi(1:1)/FCNTs (C).

3.2. Characterization of electrocatalysts

3.2.1. Structural characterization

PtNi/FCNTs, Pt/FCNTs and commercial Pt/C (E-TEK) were analyzed with ICP-OES to determine their chemical composition and metal loading, as summarized in Table 1. The total metal loading for the prepared PtNi/FCNTs and Pt/FCNTs electrocatalysts is less than the theoretical loading of 20 wt%. Also, the Pt to Ni atomic ratio varies from the nominal one except for PtNi(3:1).

The lower metal loading of all catalysts could be a result of the comparably high pH used during preparation, which however is necessary to accelerate the rate of reduction. The high pH leads to negative surface charge on the FCNTs which hinders the adsorption of negatively charged platinum ions ($PtCl_6^{2-}$) or even the negatively charged nanoparticles after their reduction due to the charge repulsion [53]. A lower metal loading however has been reported before for Pt/C and PtRu/CNTs prepared by the polyol method using EG as reducing agent at higher pH [53,54]. On the other side, as reported by Ribeiro et al. [55] a more basic environment favors Ni ion reduction. They prepared PtRuNi/C catalysts in EG at different pH and they found that at lower pH, the amount of Ni detected by EDX is very low while the metal loading was the same as in the starting precursor. With increase in the pH of the preparation media up to 11–12 the amount of Ni detected was higher but the total metal loading was 50% of its theoretical value which agrees well with our results.

The XRD patterns of the Pt/C, Pt/FCNTs and PtNi/CNTs catalysts are shown in Fig. 1. Pt/C (E-TEK) (Fig. 1A) shows diffraction peaks at 2θ of 39.9°, 46.1°, and very broad and weak signals at ca. 67.4° and 81.4°, which are characteristic for the 111, 200, 220 and 311 facets of the Pt fcc structure, respectively, while Pt/FCNTs does not show any characteristic peaks of Pt fcc which could be attributed to a small particle size of this catalyst (see below) and/or to the lower Pt loading. All PtNi/FCNTs catalysts display only the Pt 1 1 1 peak, which is slightly shifted to higher 2θ values confirming alloying formation in PtNi catalysts due to the incorporation of smaller Ni atoms into the Pt fcc lattice [27,43,56]. Importantly, the patterns for PtNi/FCNTs do not show any diffraction peak for Ni metal or its oxides while all the catalysts show a peak at about 25° 2θ which is assigned to the carbon support. No attempt was made to calculate the crystallite size of the PtNi/FCNTs catalysts from XRD due to the

Table 1
Composition (from ICP) and particle size (from TEM) for Pt/C and PtNi/FCNTs.

Catalyst sample	Pt [wt%]	Ni [wt%]	Total metal loading [wt%]	Atomic ratio Pt:Ni	Particle size from TEM [nm]
Pt/C ETEK	19.0	–	19.0	–	3.1
Pt/CNTs	04.5	–	04.5	–	1.1
PtNi(1:1)/FCNTs	11.0	1.5	12.5	2:1	2.7
PtNi(2:1)/FCNTs	09.0	0.9	09.9	3:1	2.2
PtNi(3:1)/FCNTs	06.8	0.6	07.4	3:1	2.7
PtNi(3:2)/FCNTs	09.0	0.8	09.8	3.5:1	3.0
PtNi(2:1)/FCNTs 200	–	–	–	–	3.2
PtNi(3:2)/FCNTs 400	–	–	–	–	3.9

broad, weak peaks which however point to rather small particle sizes.

XRD of the heat treated PtNi(3:1)/FCNTs and PtNi(1:1)/FCNTs electrocatalysts, respectively are shown in Fig. 1B and C.

The heat treated catalysts display more intense Pt 1 1 1 peaks and a decrease in FWHM (full width at half maximum) indicating an increase in crystallite size. The 2 0 0, 2 2 0 and 3 1 1 signals are more developed for PtNi(1:1), while PtNi(3:1) still displays only the Pt 1 1 1 signal even after heat treatment. It is important to note that with increase in the heat treatment temperature, the Pt 1 1 1 peak for PtNi/FCNTs catalysts shift to lower 2θ angle compared to of the as-prepared one, especially for those catalysts heat treated at higher temperature (400 °C). This may be attributed to a phase separation between Pt and Ni as result of nickel oxides formation during the heat treatment [57]. Note that again no peaks for Ni or Ni oxides are visible, indication either absence or very small crystallite sizes/films thickness of these species.

Selected TEM images of Pt/C ETEK, Pt/FCNTs and PtNi/FCNTs and the corresponding particle size histograms are shown in Fig. SI5. The average particle sizes calculated from counting more than 100 particles for all catalysts are listed in Table 1. Nanoparticles of Pt and PtNi are well dispersed on the support and are very small with a narrow particle size distribution. These morphological properties are one of the advantages of the polyol method used for the preparation of Pt/FCNT and PtNi/FCNTs in this work. Only the PtNi(3:2)/FCNTs show some agglomeration. The average particle size for Pt/FCNTs is very low (1.1 nm) in agreement with the absence of diffraction peaks in XRD patterns (see above). The PtNi/FCNTs catalysts show particle sizes in range of 2–3 nm. Upon heat treatment, the particle sizes increase while keeping their high dispersion.

Pt(4f) XPS spectra are presented in Fig. 2A. The Pt(4f 7/2) signal has a BE of 71.9 eV, which is close to the metal position (71 eV) [58,59]. This shift to higher energies is likely not related to a higher oxidation state of platinum but to initial-state or final-state effects due to small particle size [60,61]. In the bimetallic samples, the Pt(4f 7/2) binding energy is slightly lower (in average by ≈0.3 eV), which might indicate alloy formation. The effect is, however, near to the limits of experimental error and should not be overemphasized.

The Ni 2p spectra of selected samples are presented in Fig. 2B and C. Although the Ni signals are weak, some conclusions on the nickel state can be derived. In all samples the Ni^{2+} state with a BE of ca. 856 eV can be detected together with its satellite approximately 6 eV higher [62]. A contribution from the Ni metallic state can also be detected in the non-heat treated samples – PtNi(1:1), (2:1) and (3:1)/FCNTs. Ni appears to be almost fully oxidized in PtNi(3:1)/FCNTs 400 and the presence of metallic state is rather unclear in PtNi(2:1)/FCNTs 200. These results support the above findings from XRD that the initially present alloy, where the Ni XPS state should be more metallic, restructures during heat treatment. However the formed Ni oxides, as detected by XPS, are in a form undetectable by XRD (i.e. small particles or thin films).

The Ni content detected with XPS is lower than expected from ICP analysis. The intensity of the Ni signal is very low and the 2p 1/2 line could sometimes be barely distinguished from the background noise. Taking into account that the photo-ionization cross section for Ni is 1.5 times higher than that of Pt it can be concluded that a low amount of nickel is accessible for the XPS analysis, i.e. in the surface region of the catalyst. A possible explanation would be that a significant part was present in big particles that give small XPS intensity, contradicting however TEM and XRD results as well as XAFS results (see below). A more likely explanation would thus be that the Ni is enriched in deeper layers. The detectable Ni amount is, however, higher after heat treatment (see Table 2), in line with some segregation as speculated on from XRD results.

It is also remarkable that the Ni is strongly oxidized in the surface region. After sputtering (Fig. SI7) there is almost no more oxidized Ni. It is known that sputtering is reductive (preferential removal of O), at the same time Ni is also removed. Probably, together with a NiO layer on the outer surface of nanoparticles, separate highly dispersed NiO particles too small to be detected by XRD are present which are easily sputtered away.

Regarding the presence of oxides, it is not clear at the moment, if these form during catalyst preparation/heat treatment, or afterwards while handling the catalyst in air. However, the presence of oxides clearly indicates that not all Ni is in an alloy state in the catalyst.

Fig. 3 shows Ni K and Pt L_3 X-ray absorption near edge structure (XANES) of PtNi(1:1)/FCNT. The catalyst spectrum resembles that of NiO with most features like edge position and white line at 8337 eV. However, there is also a shoulder similar to the pre-edge feature of the metal at 8232 eV, the white line being somehow lower than that in NiO case indicates that nickel is not totally oxidized in the sample under study. The EXAFS plot for the PtNi(1:1)/FCNT (Fig. 4A) catalyst has a characteristic peak for Ni–O scattering at r = 1.68 Å. The second remarkable peak at r = 2.39 Å cannot be unambiguously identified as Ni–Ni scattering event neither in Ni metallic (ref r = 2.15 Å) nor in NiO (ref r = 2.60 Å) structures. However it can indicate the appearance of a Ni–Pt scattering event.

The catalyst Pt L_3 XANES spectrum differs slightly from that of the platinum foil (Fig. 3). The slightly more intense white line may indicate that platinum in the catalyst is somewhat oxidized, however, an electronic effect of alloy formation cannot be ruled out. Zhong and coauthors [63] also report minor white line intensification for both PtNi/C and PtCo/C systems. It was attributed to the decrease of 5d orbital filling in platinum alloys due to oxidation and hybridization. The r-space EXAFS spectrum (Fig. 4B) resembles the

Table 2
Pt to Ni atomic ratios derived from XPS data.

Preparation	Pt:Ni before He^+ sputtering	Pt:Ni after He^+ sputtering
2:1	10.2	12.2
2:1_200	5.5	–[a]
3:2	–[b]	19.7
3:1	12.4	12.3
3:1_400	3.5	7.4
1:1	6.0	8.7

[a] Strong artifact on Ni 2p signal.
[b] Too weak Ni 2p signal.

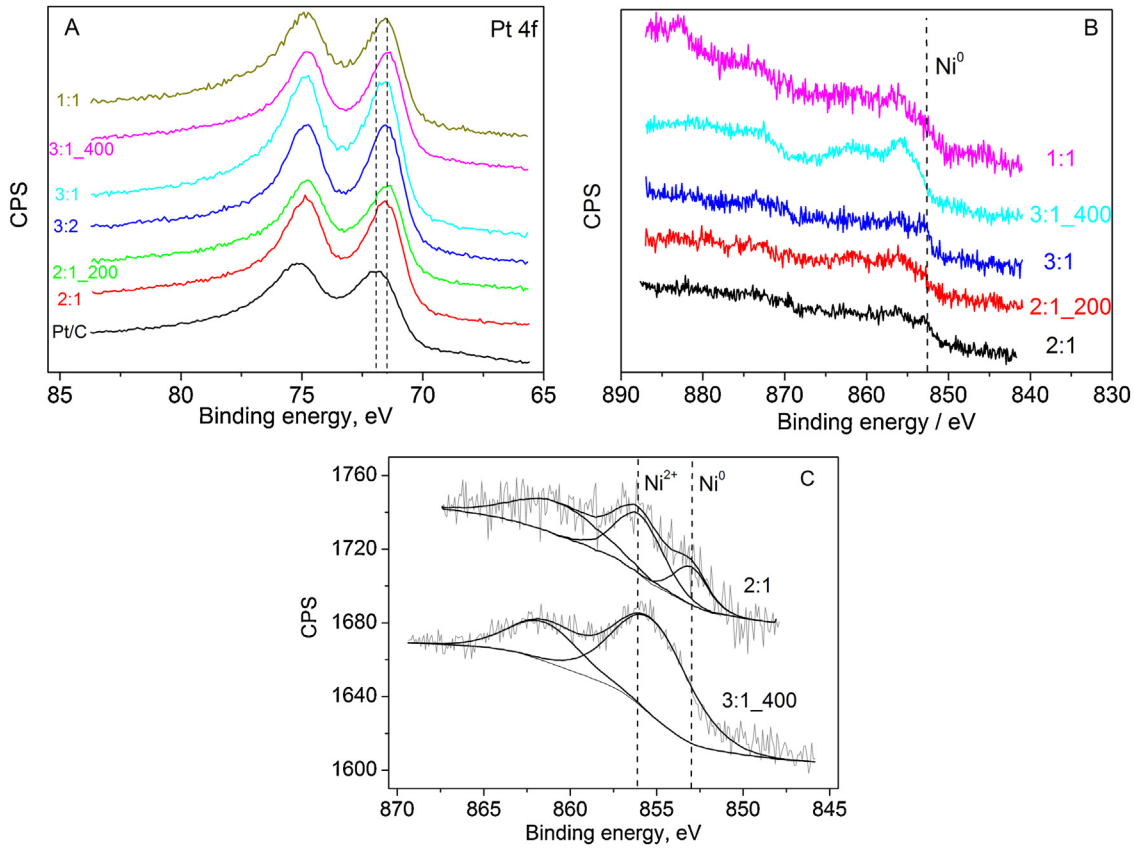

Fig. 2. XPS spectra. A – Pt 4f lines of corresponding samples; B – Ni 2p 3/2 regions; C – Ni 2p 3/2 lines with (PtNi(3:1)/FCNT 400) and without (PtNi(2:1)/FCNT) clearly detectable Ni^0 contribution.

reference platinum foil spectrum. However, the small shoulder can be detected at $r = 1.66$ Å pointing on small number of light backscatterers (presumably oxygen) presented in first coordination shell of platinum atom. Additionally, the low-r component (at ca. 2.20 Å) of the main metallic peak is more intense than it is in the reference spectrum indicating a direct contact of Pt and Ni atoms. Moreover there is a significant difference in EXAFS functions $\chi(k)$ (see Fig. 4B inset) consisting in a phase shift increasing to high k values. Thus there is a clear indication to the presence of another element but platinum in the first coordination shell.

3.2.2. Electrochemical characterization

Fig. 5 shows selected CO stripping voltammograms for PtNi(2:1)/FCNTs, PtNi(2:1)/FCNTs 200 and PtNi(2:1)/FCNTs 400, respectively; the voltammograms of the other catalysts appeared similar.

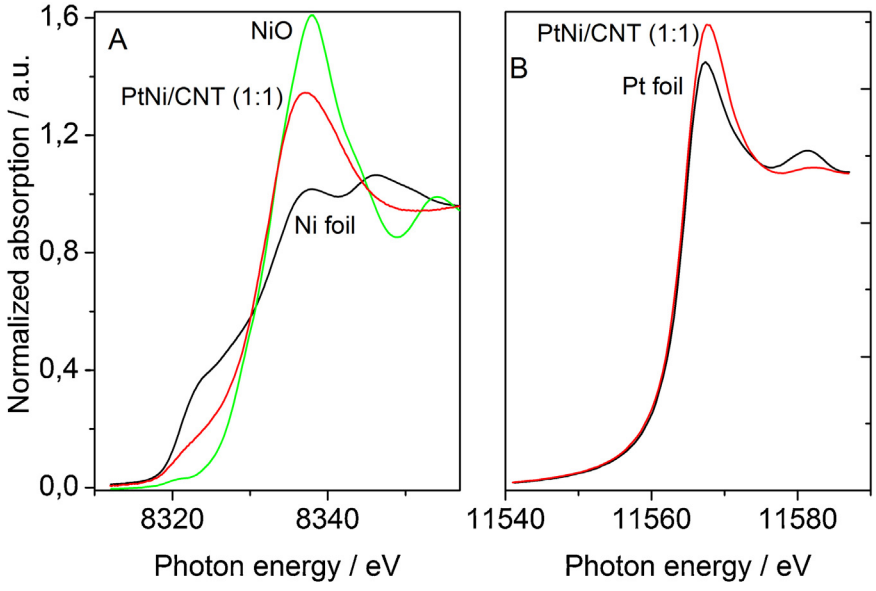

Fig. 3. Ni K (A) and Pt L_3 (B) edge XANES spectra of the PtNi(1:1)/FCNTs catalyst and reference compounds.

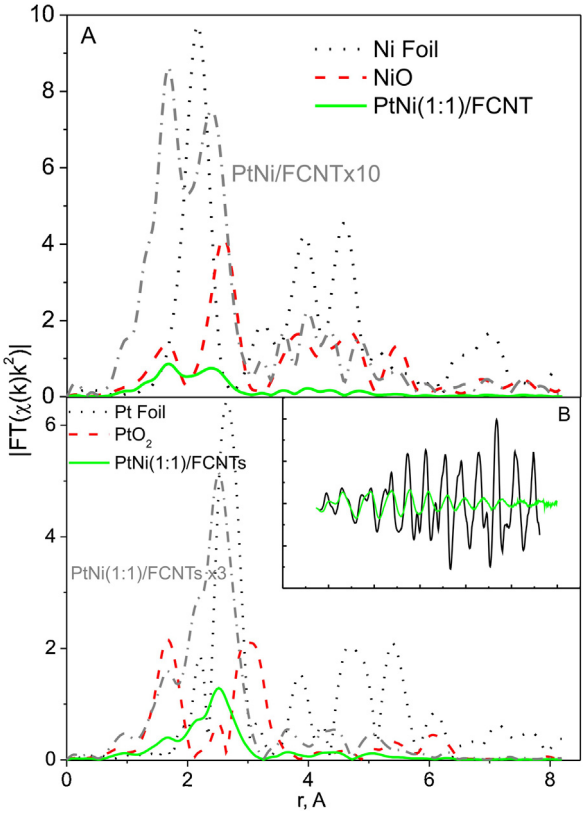

Fig. 4. A Ni K edge real space EXAFS spectra of PtNi(1:1)/FCNTs catalyst and reference compounds B Pt L3 real space EXAFS spectra of PtNi(1:1)/FCNTs catalyst, platinum foil and platinum oxide. Inset – the same spectra in *k*-space.

During the first cycle of all CVs (solid line) at potentials starting from ca. 0.5 V the adsorbed CO starts to be oxidized as evidenced by the sharp CO oxidation peak. In the second cycle (dashed line) no CO oxidation peaks are observed anymore indication that CO was oxidized completely during the first cycle. All catalysts show almost the same oxidation potential for CO oxidation except the Pt/FCNTs for which the potential is shifted slightly to higher values. The

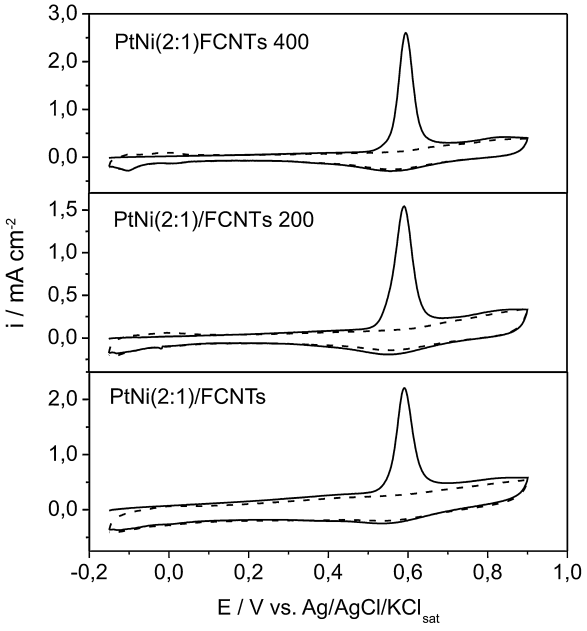

Fig. 5. CO stripping voltammograms of selected samples.

electrochemical surface area (ECSA) and specific electrochemical surface area (SECSA) for all catalysts was calculated from integration the charge passed during the oxidation of CO using the following relation [64].

$$\text{ECSA } (\text{cm}^2) = \frac{Q_{CO}\,(\text{mC})}{Q_0(\text{mC cm}^{-2})} \quad (1)$$

$$\text{SECSA } (\text{m}^2/\text{g}) = \frac{\text{ECSA}}{M_{Pt}} \quad (2)$$

where Q_{CO} is the charge passing during the CO oxidation in mC, Q_0 is the charge required for oxidation of adsorbed monolayer CO and equal to 420 (μC/cm^2) [64] and M_{Pt} is the Pt loading in the electrode.

The results are listed in Table 3. The specific electrochemical surface area is higher than that of Pt/C (E-TEK) for all prepared catalysts, except for the PtNi(1:1) sample which displays lower specific surface area of 29.08 m^2/g versus 47.20 m^2/g for Pt/C (E-TEK), which could be attributed to a higher Ni content in this catalyst as detected from ICP analysis.

In the as prepared catalysts with the exception of PtNi(1:1) all bimetallic samples display hardly any features for hydrogen adsorption/desorption in the second CV (after CO oxidation). However, after heat treatment, these features are much more pronounced, indicating the formation of a Pt enriched surface (see Fig. 5). Furthermore, for almost all PtNi/FCNTs electrocatalysts the electrochemical surface area increase with increase of heat treatment temperature while the particle size also increases as shown above with TEM. Since only surface Pt is detected during ECSA measurements and Ni is not, these results support the postulation of a more Pt-rich surface after heat treatment at 400 °C.

3.3. Structure of the catalysts

The above characterization results shall be discussed already at this part of the paper to derive a structural model of the catalyst and its changes induced by heat treatment. This model will then help to understand the results of the catalytic experiments below.

Both XPS and XAFS studies reveal that the platinum state in the catalysts under study is metallic, with clear indications of alloy formation. However, besides metallic Ni significant Ni oxide contributions are also detected, and after heat treatment oxides are the only Ni species detectable by XPS. In accordance, XRD detects the presence of alloys with the degree of alloying decreasing, however not completely vanishing, after heat treatment. Oxidic species, however, are not detected by XRD.

The difference in Pt:Ni ratio between XPS and ICP-OES results deserves special attention. While ICP-OES, analyzing the whole sample, yielded Pt:Ni ratios close to the nominal ones, XPS, restricted to the upper surface layers, indicated very high Pt:Ni ratios, the values however deceasing after heat treatment. A Ni depleted surface, with structural changes and Ni segregation however after heat treatment, is in line with this model. Thus, a PtNi alloy core surrounded by a Pt enriched shell with some Ni oxides present outside could be postulated. Further segregation occurs during heat treatment. Unfortunately the quality of XRD is not high enough to distinguish all these species due to small particle size.

The results of the electrochemical experiments are in line with these postulations. After heat treatment, Pt features are more expressed in electrochemical experiments. Heat treatment might aid in the removal of residual organic material adsorbed on the catalyst surface during the preparation process leading to an enhancement of electrochemically accessible surface (ECSA) area and development of Pt features in the CV. However, after heat treatment at 400 °C besides this simple effect of surface cleaning,

Table 3
Electrochemical parameters calculated from CO stripping measurements.

Catalysts	Peak potential for CO oxidation [V]	Charge Q [mC]	ECSA [cm^2]	SECSA [m^2/g]
Pt/C ETEK	0.60	1.346	3.20	47.2
Pt/FCNTs	0.63	0.415	0.98	61.3
PtNi/FCNTs (1:1) as prepared	0.59	0.593	1.14	29.1
PtNi/FCNTs (1:1) 200	0.59	0.609	1.45	37.0
PtNi/FCNTs (1:1) 400	0.59	0.750	1.78	45.4
PtNi/FCNTs (2:1) as prepared	0.59	0.757	1.80	56.1
PtNi/FCNTs (2:1) 200	0.59	0.612	1.45	45.2
PtNi/FCNTs (2:1) 400	0.59	0.921	2.19	68.2
PtNi/FCNTs (3:1) as prepared	0.59	0.720	1.71	70.7
PtNi/FCNTs (3:1) 200	0.59	0.710	1.69	69.8
PtNi/FCNTs (3:1) 400	0.60	0.729	1.73	71.5
PtNi/FCNTs (3:2) as prepared	0.59	0.981	2.33	72.6
PtNi/FCNTs (3:2) 200	0.58	0.782	1.86	57.9
PtNi/FCNTs (3:2) 400	0.59	0.780	1.85	57.6

characterization indicates changes in the catalyst, i.e. more oxidized Ni species and a reduction in the degree of alloying (see XRD). Obviously a Pt enriched surface or separated phases of Pt and Ni(oxides) render the voltammograms more Pt characteristic than a PtNi surface [63]. While this effect is strong in the catalyst with high Ni content (PtNi(1:1) (real ratio was 2:1), it is less pronounced in the catalysts (2:1) and (3:1) (both real ratio 3:1), where also particle growth diminishes the effect of ECSA enhancement. The decrease of electrochemical surface area upon heat treatment in the PtNi (3:2) could in line with this be attributed to agglomeration and growth of nanoparticles, as indicated by TEM and which overcompensates the other changes in the catalyst.

To further analyze the structural features of the catalyst, EXAFS functions were fitted with three shell model using backscattering amplitudes and phases theoretically calculated by ab-initio FEFF8.10 code [45]. For the Ni K edge the Ni–Ni homo- and Ni–Pt heterometallic scattering contributions were used together with one metal-oxygen shell. The Pt L_3 edge was fitted using Pt–Pt and Pt–Ni contributions. The fitting results, consisting of coordination number (CN), scattering distance (r), Debye–Waller factors index of power (σ^2) and muffin-tin potential adjustment (ΔE) are presented in Table 4 for the Pt L_3 and Table 5 for the Ni K edge respectively. It can be seen that platinum tends to form homoatomic agglomerates where every atom has ca. 5 Pt neighbors. Pt–Ni scattering events however can be also detected with the average coordination number of 1.3. The presence of Pt–Ni alloy structure is thus numerically proven. Additionally, the fact that the total coordination numbers of both Pt (6.7) and Ni (5.6) are close to each other indicates that no enclosed (like core–shell) structure has been formed. To study Pt–Ni alloying extent, the method suggested by Hwang et al. [65] was used. In the method, the degree of alloying is determined by calculating heteroatomic bonding probability from coordination numbers derived from the EXAFS fit procedure and relating them subsequently to the theoretical values dictated by the alloy stoichiometry. For binary alloys, 7 boundary cases were suggested, including separated and perfect alloys as well as structures of various degrees of homogeneity. The method can be applied also for our case where some Ni–O coordinations are present because it relies entirely on ratios of coordination numbers. In case of the Pt:Ni (1:1) catalyst, the relative extent of alloying of platinum (J_{Pt}) was calculated to be 60, whereas J_{Ni} is close to 100. According to the Hwang classification this indicates that Ni atoms are tending to form homophilic structures close to the outer surface of the nanoparticles (Ni-rich shell, Pt-rich core). The latter however contradicts the low Ni 2p XPS line intensities. We suspect that the homophilic structures of nickel atoms in the alloy particles are concentrated in regions near the support so that they are shielded from the atmosphere and at the same time less visible for XPS. A structural model can be suggested as shown in Fig. 6. This model represents both the as prepared and heat treated samples, which however differ in the amount of surface segregation. The alloyed Ni exposed to the atmosphere is oxidized. The alloy particles probably coexist with very small segregated NiO aggregates which enhance the predominance of oxidized Ni in the XPS spectra.

A tentative explanation for the formation of such structures might be that the positively charged Ni^{2+}-ions do adsorb on the surface of the FCNTs, which are likely negatively charged at positive pH, while the negatively charged $PtCl_6^{2-}$-ions do not. Initially formed Ni clusters on the FCNTs surface then catalyze the further reduction of Pt and Ni and lead to the formation of a Pt-rich alloy surrounding the Ni-rich core attached to the CNT.

3.4. Methanol electrooxidation

After having established the structure of the catalysts and the changes induced by heat treatment, it would be highly interesting to study the behavior of these materials as catalysts for the electrooxidation of methanol. Cyclic voltammograms for methanol oxidation in 0.5 M H_2SO_4 are shown in Fig. 7, showing the typical behavior for Pt and Pt based catalysts in sulfuric acid solution containing methanol [66–71].

The ratio between the peak current in the forward (I_f) and the backward scan (I_b) is usually taken as the measure for the tolerance of the catalyst against CO poisoning with a higher I_f:I_b indicating higher tolerance. Fig. 7 demonstrates that the catalyst with 2:1 and

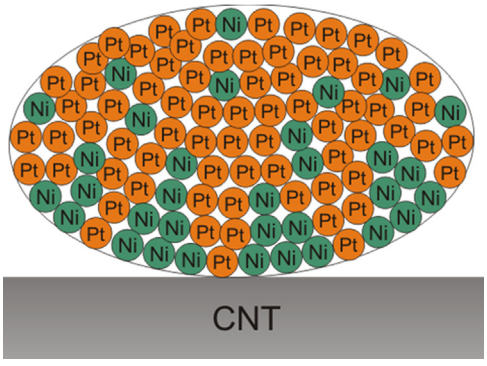

Fig. 6. Schematic sketch of bimetallic Pt–Ni nanoparticles demonstrating that Pt and Ni are not randomly distributed in the particle, but Ni is enriched near the support and Pt toward the gas phase. Model represents both as prepared and heat treated samples, which however differ in the amount of surface segregation.

Table 4
Pt L3 edge best-fit results within two shell model.

Reference path	r (Å)	CN	$\sigma^2 \times 10^{-3}$ (Å^2)	ΔE (eV)
Pt–Ni = 2.6165	2.65 ± 0.02	1.32 ± 0.20	7.49 ± 1.47	15.13 ± 2.56
Pt–Pt = 2.6976	2.71 ± 0.01	5.31 ± 0.34	6.99 ± 0.46	10.19 ± 0.36

ΔR = 2.05 Å; Δk = 2.77–15.83 Å^{-1}. Errors are assumed to be proportional to $k^{1.5}$, Pt–Ni distance is constrained between 2.5 and 2.7 Å.

Table 5
Ni K edge best-fit results within three shell model.

Reference path	r (Å)	CN	$\sigma^2 \times 10^{-3}$ [Å^2]	ΔE [eV]
Ni–O = 2.0842	2.04 ± 0.01	2.19 ± 0.30	6.74 ± 2.03	4.43 ± 1.37
Ni–Pt = 2.6165	2.64 ± 0.02	2.25 ± 1.02	8.56 ± 2.70	−3.68 ± 0.91
Ni–Ni = 2.6976	2.63 ± 0.06	1.14 ± 0.23	8.86 ± 2.99	3.33 ± 6.27

ΔR = 2.43 Å; Δk = 3.35–15.83 Å^{-1}. Errors are assumed to be proportional to k.

3:1 nominal Pt:Ni ratios (the actual Pt:Ni ratios for theses catalysts are 3:1) display a higher I_f:I_b which reflects their higher CO tolerance. On the other hand, the catalysts 3:2 and 1:1 exhibit a somewhat higher current in the reverse peak indicating a slightly higher susceptibility to CO poisoning. A Pt:Ni ratio of 3:1 might thus be optimum in terms of CO tolerance. However, the differences between these samples are comparably small. All prepared catalysts show superior CO tolerance and methanol oxidation compared to the commercial sample. In general we can say that the presence of Ni and/or its oxides has a beneficial role affecting the CO tolerance during the MOR. On the other hand, the higher CO tolerance of Pt/FCNTs indicated by the lower current in the reverse peak could be attributed to the small particles of this catalyst which would be more active for CO oxidation. Upon the heat treatment, formation of a Pt enriched surface is observed which displays methanol oxidation behavior similar to that of Pt/C ETEK with higher currents in the reverse scan (not shown).

From the CVs, the mass specific activity, which is defined as the current at the peak oxidation potential in the forward scan divided by Pt loading on the electrode, was determined. The values for mass specific activity, surface specific activity and peak potential are listed in Table 6.

All PtNi/FCNTs show higher mass specific activity (which is relevant for fuel cell application form the viewpoint of costs) than the commercial Pt/C (E-TEK) except for PtNi(1:1), which exhibits activity very close to the commercial catalyst. However, Pt/FCNTs provide the lowest activity among all catalysts which probably can be attributed to the very small particle size of this catalysts (1.1 nm), and thus a decreased number of ensemble sites for methanol adsorption on their surface leading to lower activity [4]. For PtNi(2:1), PtNi(3:1) and PtNi(3:2) catalysts, the activities are close to each other, which is not surprising as theses catalysts posses similar atomic Pt to Ni ratios of 3:1 as determined with ICP-OES analysis, with PtNi(3:1) providing the highest activity among

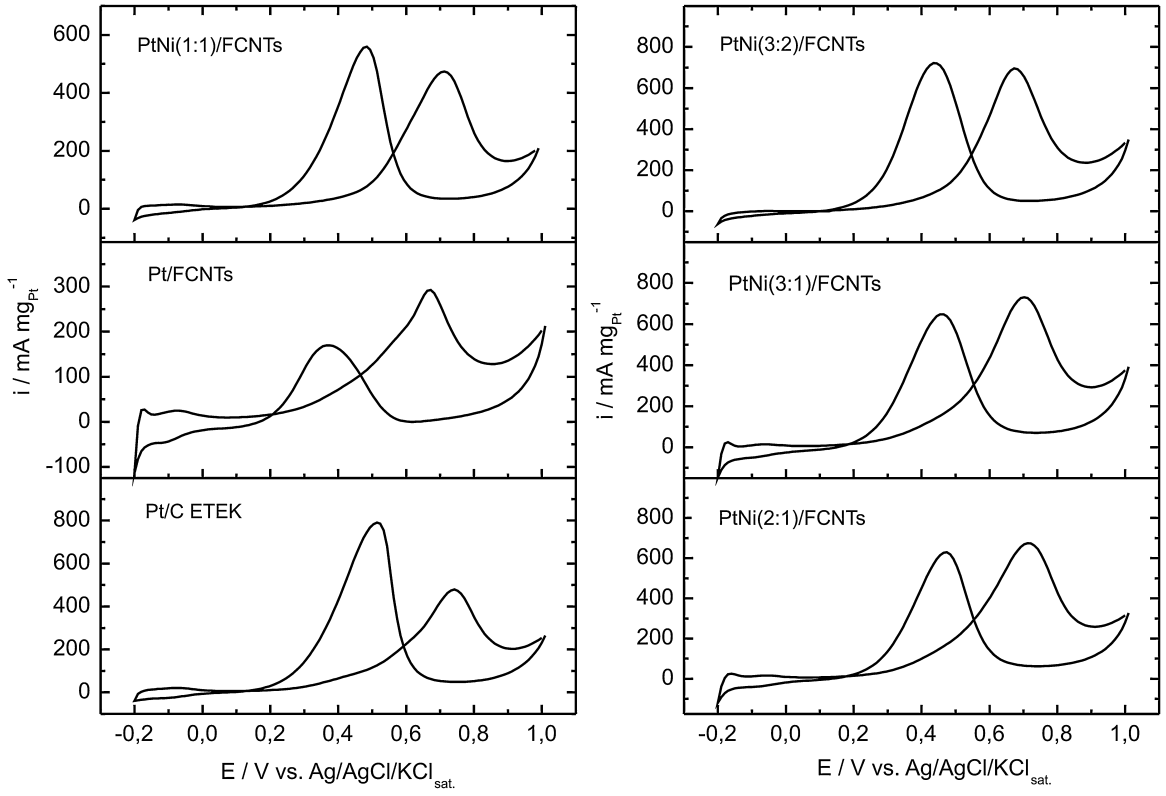

Fig. 7. CV of Pt/C ETEK, Pt/FCNTs and PtNi/FCNTs electrocatalysts in 0.5 M H_2SO_4/1 M CH_3OH (scan rate 20 mV/s). The current was normalized to the mass of Pt in the electrode.

Table 6
Electrochemical parameters calculated from cyclic voltammetry measurements.

Catalysts	Peak potential [V]	Surface specific activity [mA/cm^2)]	Mass specific activity [mA/mg$_{Pt}$]
Pt/C ETEK	0.742	1.00	478.2
Pt/FCNTs	0.668	0.47	292.9
PtNi/FCNTs (1:1) as prepared	0.714	1.62	474.2
PtNi/FCNTs (1:1) 200	0.685	1.37	508.9
PtNi/FCNTs (1:1) 400	0.714	0.87	395.6
PtNi/FCNTs (2:1) as prepared	0.715	1.20	675.3
PtNi/FCNTs (2:1) 200	0.675	1.27	575.1
PtNi/FCNTs (2:1) 400	0.715	0.77	530.5
PtNi/FCNTs (3:1) as prepared	0.705	1.04	730.3
PtNi/FCNTs (3:1) 200	0.678	1.20	841.3
PtNi/FCNTs (3:1) 400	0.668	0.83	588.8
PtNi/FCNTs (3:2) as prepared	0.677	0.97	694.3
PtNi/FCNTs (3:2) 200	0.675	1.10	648.7
PtNi/FCNTs (3:1) 400	0.697	0.86	496.4

all catalysts. Additionally, the mass specific activities found by us are higher than those reported in the literature [72,73].

The order of activity changes if the surface specific activity is considered (i.e. the peak potential related to the surface area determined with CO stripping) (CVs see Fig. SI6). As summarized in Table 6, the activity is highest in the catalyst with highest Ni content and decreases with Ni content. The virtual discrepancy between surface and mass specific activities certainly relates to the fact that the surface specific activities are related to the Pt atoms available at the surface only, which depends on particle size, Pt:Ni ratio, etc. I.e. the individual Pt atoms at the surface of PtNi(1:1)/FCNT are obviously in average more active, but likely there are less of them leading to low mass specific activities, the lower SSA of our catalysts compared to literature values [72] might be due to the fact that we used CO stripping to determine surface areas whereas in the literature H adsorption desorption has been used. It is well known that the former yields higher surface areas [74] which might in part help to explain the lower SSA.

It is known that at least three adjacent Pt sites in the proper spatial arrangement are required in the methanol chemisorptions step [75]. Furthermore, poisoning CO has to be oxidized following either the electronic effect or the bifunctional mechanism. We assume that the arrangement of Pt to Ni on the surface of catalysts and therefore the population of Pt active site is the major factor determining the activity of PtNi catalysts for methanol oxidation also in our case. However, from our results it is hard to decide whether enhanced CO oxidation via the bifunctional mechanism or by an electronic effect occurs. The former is tentatively excluded since no early peak for CO oxidation is observed in the CO stripping voltammograms. The latter should however be taken into consideration since from the XPS results a shift in binding energy, although minor in nature, has been observed.

Other factors such as the particle size and the dispersion of the nanoparticles certainly additionally play a significant role determining catalytic activity. Also, the presence of oxygen functional groups on the surface of support could enhance the methanol oxidation on the catalysts surface through oxygen supply which facilitate the oxidation of adsorbed CO [37,46].

Heat treatment at 200 °C results in higher catalytic activity for most of the PtNi/FCNTs in terms of mass activity and peak potential than the as prepared catalyst (Table 6) which can be attributed to a cleaning of the catalyst surface from adsorbed organic residuals, making more active sites available for methanol oxidation.

However, after treatment at 400 °C the surface and mass specific catalytic activity decreases dramatically for all catalysts. This can be attributed to the catalyst restructuring upon heat treatment as discuss above from CV, XRD, XPS and XAFS. Obviously this restructuring with the concomitant surface Pt-enrichment leads to a decrease in the population of highly active sites on the surface and probably changes the reaction mechanism [76]. Differences in CO poisoning are likely not responsible given the similar CO oxidation potentials in all catalysts.

Besides activity, stability of a catalyst is also a decisive factor in determining its suitability for real DMFC applications. The initial stability of PtNi catalysts has been studied by performing 200 repetitive cycles in 0.5 M H_2SO_4/1 M CH_3OH.

Fig. 8A shows the CV of selected cycle numbers for PtNi(3:1)/FCNTs. During the potential cycling, the current decreases slightly with increasing cycle number. Meanwhile, the CVs for PtNi(3:1)/FCNTs 400 (Fig. 8B) show a different behavior.

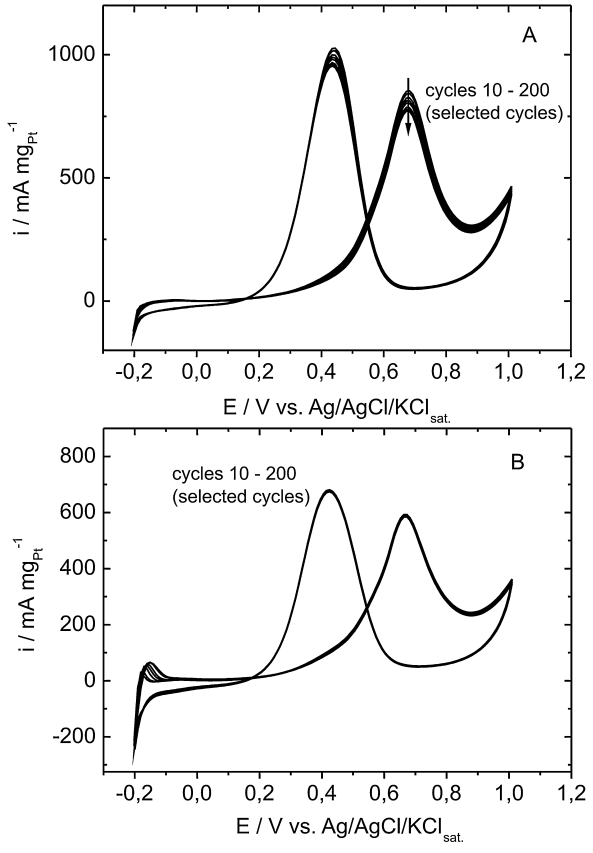

Fig. 8. CV of PtNi(3:1)/FCNTs 200 (A) and PtNi(3:1)/FCNTs 400 (B) electrocatalysts in 0.5 M H_2SO_4/1 M CH_3OH (scan rate 100 mV/s).

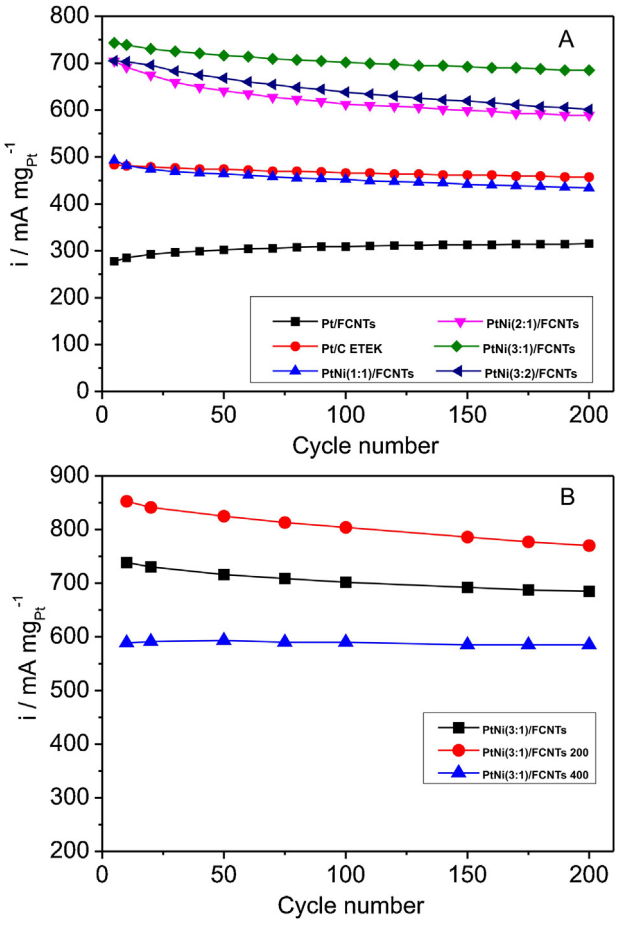

Fig. 9. Variation of mass activity (mA/mg$_{Pt}$) with the number of cycle during the cycling potential, the data obtained for all catalysts from CV in 0.5 M H_2SO_4/1 M CH_3OH, scan rate 0.1 V/s for 200 cycle in potential window (−0.2 to 1 V, vs. Ag/AgCl).

The characteristic peaks for hydrogen adsorption/desorption are more developed in comparison to those for PtNi(3:1)/FCNTs and PtNi(3:1)/FCNTs 200 even in presence of methanol and these peaks further develop with increasing cycle number, in line with the observations form CO stripping showing more expressed Pt characteristics in the heat treated samples. The catalytic activity shows high stability with almost no change during the 200 cycles.

This behavior is visualized in Fig. 9A, which shows the variation of current with the cycle number up to 200 cycles for as prepared PtNi/FCNTs. This figure indicates the long term stability for PtNi/FCNTs catalysts: PtNi(3:1) retains 92.2% from its initial current at cycle 5 after 200 cycles. On the other side, although the catalysts subjected to heat treatment at higher temperature (400 °C) showed lower activity than the as prepared ones and those after heat treatment at 200 °C, they show very high stability upon cycling up to 200 cycles. Fig. 9B shows the variation of current with the number of cycle for the as prepared PtNi(3:1) in comparison to the heat treated one. After heat treatment at 400 °C the catalyst kept its initial activity within the limits of experimental error over 200 cycles in comparison with a retained current of 92.2% for the as-prepared one and 90% for the one heat treated at 200 °C. Decrease in activity during cycling might be to Ni dissolution and/or restructuring, which does not occur in the already segregated samples treated at 400 °C, which are thus more stable.

These features discussed above make the PtNi catalysts system with a proper surface concentration one of the most active catalysts for long-term methanol fuel cells.

4. Conclusion

PtNi/FCNTs with different Pt:Ni ratios have been prepared with ethylene glycol as reducing agent (polyol method). The catalysts display the Pt fcc structure with indications for alloy formation but also proofs for the presence of Ni oxides. Heat treatment at 400 °C in N_2 atmosphere resulted in phase separation/restructuring of the catalysts. A model is suggested where Ni-rich phases form close to the FCNTs which are surrounded by a Pt-rich alloy. It is important to mention that only the combination of advanced characterization techniques including XAS, XRD, TEM and XPS allowed to unravel the intricacies of the structures synthesized which would not have been possible from a single or two techniques alone. The highest catalytic activity was found for a Pt/Ni ratio of 3, which could be attributed to the availability and proper population of active Pt sites required for methanol adsorption in this catalyst and the easy removal of intermediate CO. Phase separation by heat treatment leads lower catalytic activity.

Acknowledgments

AB.A.A. Nassr gratefully acknowledges a scholarship from the Ministry of Higher Education and Scientific Research (MHESR), Egypt and German Academic Exchange Service (DAAD), Germany, within the program German Egyptian Research Long-Term Scholarship (GERLS) to pursue his PhD studies at Martin-Luther-University Halle-Wittenberg. Dr. F. Heyroth from the Interdisciplinary Centre of Materials Science is gratefully acknowledged for performing TEM measurements. J. Bienias from our institute at Martin-Luther-University is acknowledged for performing BET and TGA measurements. We acknowledge access to XRD facilities of our inorganic chemistry department and Eik Koslowski for performing the measurements.

Appendix A. Supplementary data

Supplementary material related to this article can be found, in the online version, at http://dx.doi.org/10.1016/j.apcatb.2013.06.013.

References

[1] E.L. Gyenge, in: J. Zhang (Ed.), PEM Fuel Cell Electrocatalysts and Catalyst Layers: Fundamentals and Applications, Springer, New York, 2008, pp. 165–270.
[2] A.S. Aricò, S. Srinivasan, V. Antonucci, Fuel Cells 1 (2001) 133–161.
[3] A.S. Aricò, V. Baglio, V. Antonucci, in: H. Liu, J. Zhang (Eds.), Electrocatalysis of Direct Methanol Fuel Cells: From Fundamentals to Applications, Wiley-VCH, 2009, pp. 1–77.
[4] Y. Tang, L. Zhang, Y. Wang, Y. Zhou, Y. Gao, C. Liu, W. Xing, T. Lu, Journal of Power Sources 162 (2006) 124–131.
[5] R. Ganesan, D.J. Ham, J.S. Lee, Electrochemistry Communications 9 (2007) 2576–2579.
[6] M. Li, S. Zhao, G. Han, B. Yang, Journal of Power Sources 191 (2009) 351–356.
[7] O.V. Cherstiouk, P.A. Simonov, E.R. Savinova, Electrochimica Acta 48 (2003) 3851–3860.
[8] D. Jun Guo, S.-K. Cui, Journal of Solid State Electrochemistry 12 (2008) 1393–1397.
[9] J.L. Lu, Z.H. Li, S.P. Jiang, P.K. Shen, L. Li, Journal of Power Sources 202 (2012) 56–62.
[10] J. Kim, S.M. Choi, S.H. Nam, M.H. Seo, S.H. Choi, W.B. Kim, Applied Catalysis B 82 (2008) 89–102.
[11] T. Maiyalagan, T.O. Alaje, K. Scott, Journal of Physical Chemistry C 116 (2012) 2630–2638.
[12] H. Zhang, X. Xu, P. Gu, C. Li, P. Wu, C. Cai, Electrochimica Acta 56 (2011) 7064–7070.
[13] L. Feng, G. Gao, P. Huang, X. Wang, C. Zhang, J. Zhang, S. Guo, D. Cui, Nanoscale Research Letters 6 (2011) 551–560.
[14] Y.Q. Wang, Z.D. Wei, L. Li, M.B. Ji, Y. Xu, P.K. Shen, J. Zhang, H. Zhang, Journal of Physical Chemistry C 112 (2008) 18672–18676.
[15] S. Papadimitriou, S. Armyanov, E. Valova, A. Hubin, O. Steenhaut, E. Pavlidou, G. Kokkinidis, S. Sotiropoulos, Journal of Physical Chemistry C 114 (2010) 5217–5223.

[16] R. Lin, C. Cao, H. Zhang, H. Huang, J. Ma, International Journal of Hydrogen Energy 37 (2012) 4648–4656.
[17] E. Lee, A. Manthiram, Journal of Physical Chemistry C 114 (2010) 21833–21839.
[18] D.R. Ou, T. Mori, H. Togasaki, M. Takahashi, F. Ye, J. Drennan, Langmuir 27 (2011) 3859–3866.
[19] B.Y. Xia, S. Ding, Ha.B. Wu, X. Wang, X. Wen, RSC Advances 2 (2012) 792–796.
[20] P. Justin, P.H.K. Charan, G.R. Rao, Applied Catalysis B: Environmental 100 (2010) 510–515.
[21] H. Yuan, D. Guo, X. Qiu, W. Zhu, L. Chen, Journal of Power Sources 188 (2009) 8–13.
[22] H. Liu, D. Xia, J. Zhang, in: J. Zhang (Ed.), PEM Fuel Cell Electrocatalysts and Catalyst Layers: Fundamentals and Applications, Springer, New York, 2008, pp. 631–654.
[23] X. Zhao, M. Yin, L. Ma, L. Liang, C. Liu, J. Liao, T. Lu, W. Xing, Energy and Environmental Science 4 (2011) 2736–2753.
[24] P.P. Lopes, K.S. Freitas, E.A. Ticianelli, Electrocatalysis 1 (2010) 200–212.
[25] M. Watanabe, S. Motoo, Journal of Electroanalytical Chemistry 60 (1975) 275–283.
[26] T. Frelink, W. Visscher, J.A.R. van Veen, Surface Science 335 (1995) 353–360.
[27] K.-W. Park, J.-H. Choi, B.-K. Kwon, S.-A. Lee, Y.-E. Sung, H.-Y. Ha, S.-A. Hong, H. Kim, A. Wieckowski, Journal of Physical Chemistry B 106 (2002) 1869–1877.
[28] Q. Jiang, L. Jiang, H. Hou, J. Qi, S. Wang, G. Sun, Journal of Physical Chemistry C 114 (2010) 19714–19722.
[29] R. Chetty, S. Kundu, W. Xia, M. Bron, W. Schuhmann, V. Chirila, W. Brandl, T. Reinecke, M. Muhler, Electrochimica Acta 54 (2009) 4208–4215.
[30] A.B. Kashyout, A.B.A.A. Nassr, L. Giorgi, T. Maiyalagan, B.A.B. Youssef, International Journal of Electrochemical Science 6 (2011) 379–393.
[31] X. Wang, H. Wang, R. Wang, Q. Wang, Z. Lei, Journal of Solid State Electrochemistry 16 (2012) 1049–1054.
[32] E. Lee, A. Murthy, A. Manthiram, Journal of Electroanalytical Chemistry 659 (2011) 168–175.
[33] J. Zeng, J.Y. Lee, Journal of Power Sources 140 (2005) 268–273.
[34] C.-T. Hsieh, J.-Y. Lin, Journal of Power Sources 188 (2009) 347–352.
[35] N.P. Lebedeva, G.J.M. Janssen, Electrochimica Acta 51 (2005) 29–40.
[36] P. Hernández-Fernández, M. Montiel, P. Ocón, J.L.G. Fierro, H. Wangc, H.D. Abruna, S. Rojas, Journal of Power Sources 195 (2010) 7959–7967.
[37] R.S. Amina, K.M. El-Khatib, R.M. Abdel Hameed, E.R. Souaya, M.A. Etman, Applied Catalysis A 407 (2011) 195–203.
[38] T.C. Deivaraj, W. Chena, J.Y. Lee, Journal of Materials Chemistry 13 (2003) 2555–2560.
[39] Q. Jiang, L. Jiang, S. Wang, J. Qi, G. Sun, Catalysis Communications 12 (2010) 67–70.
[40] A.A. El-Shafei, Journal of Electroanalytical Chemistry 471 (1999) 89–95.
[41] R. Manoharan, J.B. Goodenough, Journal of Materials Chemistry 2 (1992) 875–887.
[42] Y. Liang, H. Zhang, Z. Tian, X. Zhu, X. Wang, B. Yi, Journal of Physical Chemistry B 110 (2006) 7828–7834.
[43] S. Jiang, Y. Ma, H. Tao, G. Jian, X. Wang, Y. Fan, J. Zhu, Z. Hu, Journal of Nanoscience and Nanotechnology 10 (2010) 3895–3900.
[44] K.V. Klementiev, Journal of Physics D: Applied Physics 34 (2001) 209–217 www.cells.es/Beamlines/CLAESS/software/viper.html
[45] A.L. Ankudinov, B. Ravel, J.J. Rehr, S.D. Conradson, Physical Review B 58 (1998) 7565–7576.
[46] P. Hernandez-Fernandez, S. Baranton, S. Rojas, P. Ocon, J.-M. Leger, J.L.G. Fierro, Langmuir 27 (2011) 9621–9629.
[47] J.L. Figueiredo, M.F.R. Pereira, M.M.A. Freitas, J.J.M. Orfao, Carbon 37 (1999) 1379–1389.
[48] W. Xia, Y. Wang, R. Bergstraßer, S. Kundu, M. Muhler, Applied Surface Science 254 (2007) 247–250.
[49] A.E. Aksoylu, M. Madalena, A. Freitas, M. Fernando, R. Pereira, J.L. Figueiredo, Carbon 39 (2001) 175–185.
[50] D.Z. Mezalira, L.D. Probst, S. Pronier, Y. Batonneau, C. Batiot-Dupeyrat, Journal of Molecular Catalysis A 340 (2011) 15–23.
[51] W. Zhang, J. Chen, G.F. Swiegers, Z.-F. Mab, G.G. Wallace, Nanoscale 2 (2010) 282–286.
[52] R. Kannan, U. Bipinlal, S. Kurungot, V.K. Pillai, Physical Chemistry Chemical Physics 13 (2011) 10312–10317.
[53] H.-S. Oh, J.-G. Oh, Y.-G. Hong, H. Kim, Electrochimica Acta 52 (2007) 7278–7285.
[54] L. Ren, Y. Xing, Electrochimica Acta 53 (2008) 5563–5568.
[55] V.A. Ribeiro, O.V. Correa, A.O. Neto, M. Linardi, E.V. Spinace, Applied Catalysis A 372 (2010) 162–166.
[56] H. Wu, D. Wexler, G. Wang, Journal of Alloys and Compounds 488 (2009) 195–198.
[57] T.-Y. Jeon, S.J. Yoo, Y.-H. Cho, K.-S. Lee, S.H. Kang, Y.-E. Sung, Journal of Physical Chemistry C 113 (2009) 19732–19739.
[58] G. Johansson, J. Hedman, A. Berndtsson, M. Klasson, R. Nilsson, Journal of Electron Spectroscopy and Related Phenomena 2 (1973) 295–317.
[59] S.D. Cameron, D.J. Dwyer, Surface Science 176 (1986) L857–L860.
[60] M.G. Manson, Physical Review B 27 (1983) 748–762.
[61] G.K. Wertheim, S.B. Dicenzo, S.E. Youngquist, Physical Review Letters 51 (1983) 2310–2313.
[62] L.A. Feldkamp, L.C. Davis, Physical Review B 22 (1980) 3644–3653.
[63] R. Loukrakpam, J. Luo, T. He, Y. Chen, Z. Xu, P.N. Njoki, B.N. Wanjala, B. Fang, D. Mott, J. Yin, J. Klar, B. Powell, C.-J. Zhong, Journal of Physical Chemistry C 115 (2011) 1682–1694.
[64] M.V. Martınez-Huerta, S. Rojas, J.L. Gomez de la Fuente, P. Terreros, M.A. Pena, J.L.G. Fierro, Applied Catalysis B 69 (2006) 75–84.
[65] B.-J. Hwang, L.S. Sarma, J.-M. Chen, C.-H. Chen, S.-C. Shih, G.-R. Wnag, D.-G. Liu, J.-F. Lee, M.-T. Tang, Journal of the American Chemical Society 127 (2005) 11140–11145.
[66] H.-Y. Lee, W. Vogel, P.P.-J. Chu, Langmuir 27 (2011) 14654–14661.
[67] J. Prabhuram, T.S. Zhao, Z.K. Tang, R. Chen, Z.X. Liang, Journal of Physical Chemistry B 110 (2006) 5245–5252.
[68] Z. Liu, F. Su, X. Zhang, S.W. Tay, ACS Applied Materials & Interfaces 3 (2011) 3824–3830.
[69] L. Ma, X. Zhao, F. Si, C. Liua, J. Liaoa, L. Lianga, W. Xing, Electrochimica Acta 55 (2010) 9105–9112.
[70] Y.-Y. Chu, Z.-B. Wang, Z.-Z. Jiang, D.-M. Gu, G.-P. Yin, Fuel Cells 10 (2010) 914–919.
[71] Z. Sun, X. Wang, Z. Liu, H. Zhang, P. Yu, L. Mao, Langmuir 26 (2010) 12383–12389.
[72] C. Xu, J. Hou, X. Pang, X. Li, M. Zhu, B. Tang, International Journal of Hydrogen Energy 37 (2012) 10489–10498.
[73] B. Lu, S. Xu, X. Yan, Q. Xue, Electrochemistry Communications 23 (2012) 72–75.
[74] K.J.J. Mayrhofer, D. Strmcnik, B.B. Blizanac, V. Stamenkovic, M. Arenz, N.M. Markovic, Electrochimica Acta 53 (2008) 3181–3188.
[75] H.A. Gasteiger, N. Markov, P.N. Ross Jr., E.J. Cairns, Journal of Physical Chemistry 97 (1993) 12020–12029.
[76] P. Hernandez-Fernandez, S. Rojas, P. Ocon, A. de Frutos, J.M. Figueroa, P. Terreros, M.A. Pena, J.L.G. Fierro, Journal of Power Sources 177 (2008) 9–16.